Supplementary Material

Generalized Integral Transform Modeling of Complex Coupled-Field Transport in Two-Dimensional Keller–Segel Chemotaxis: Verification, Spectral Convergence, and Self-Similar Localization

S1 Additional one-dimensional convergence and verification results

The main manuscript reports both U- and V-field convergence and direct GITT–FVM/MOL comparisons. This section provides complementary truncation data, additional times, self-convergence evidence, and detailed error diagnostics.

Table S1: One-dimensional GITT errors at $t = 3$ for $N = 32$ relative to $N = 64$.

χ	$E_{\infty,U}$	$E_{2,U}$	$E_{\infty,V}$	$E_{2,V}$
1	2.802×10^{-10}	2.781×10^{-10}	7.572×10^{-10}	7.546×10^{-10}
2	9.607×10^{-11}	9.228×10^{-11}	2.101×10^{-10}	2.092×10^{-10}
3	2.046×10^{-10}	2.259×10^{-10}	3.657×10^{-10}	3.716×10^{-10}
4	1.050×10^{-10}	1.017×10^{-10}	6.257×10^{-11}	5.973×10^{-11}
5	1.449×10^{-8}	1.778×10^{-8}	1.423×10^{-10}	8.050×10^{-11}

Table S2: Reference-free one-dimensional FVM self-convergence orders at $t = 3$ for the $M = 400, 800, 1600$ grid sequence.

χ	$p_{\infty,U}$	$p_{2,U}$	$p_{\infty,V}$	$p_{2,V}$
1	1.999992	1.999991	2.000006	2.000006
2	1.999989	1.999986	1.999996	1.999994
3	1.999972	1.999986	1.999993	1.999988
4	1.999975	1.999982	2.000001	1.999997
5	2.000121	2.000113	2.000108	2.000072

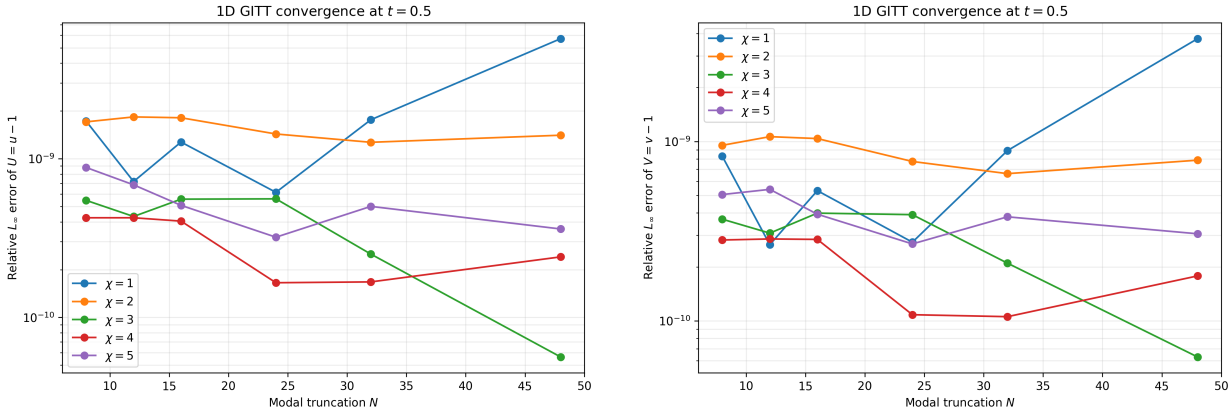


Figure S1: One-dimensional GITT convergence at $t = 0.5$: U (left) and V (right).

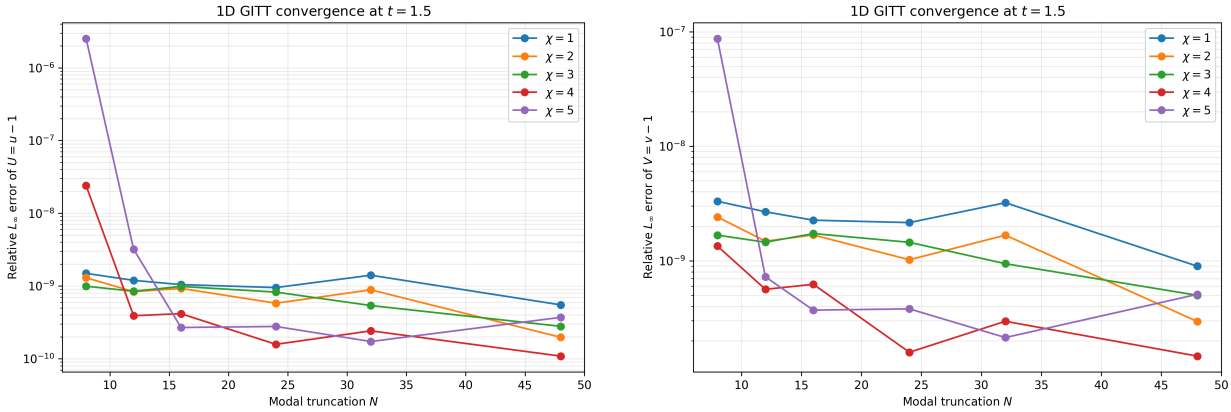


Figure S2: One-dimensional GITT convergence at $t = 1.5$: U (left) and V (right).

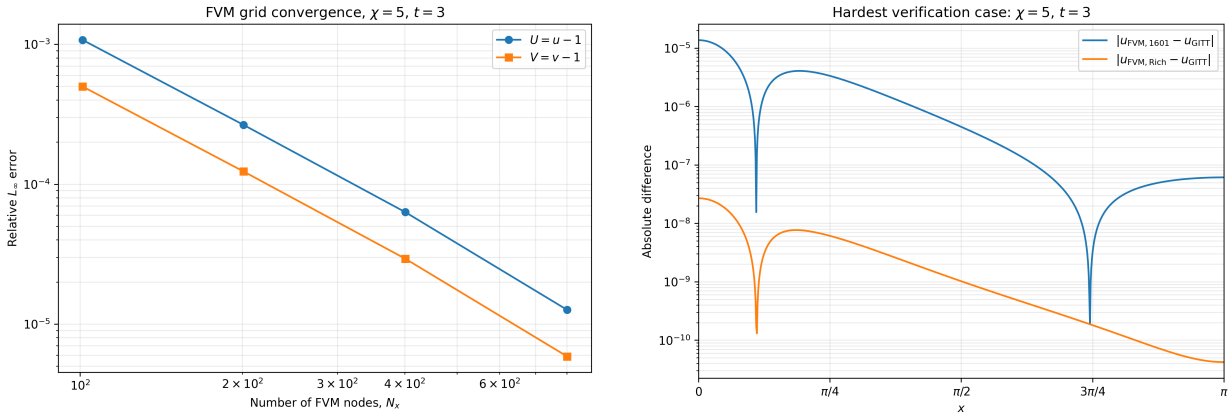


Figure S3: Independent one-dimensional FVM verification for $\chi = 5$, $t = 3$: grid convergence (left) and direct/Richardson difference relative to GITT (right).

S2 Additional one-dimensional parametric profiles

The following profiles complement the $t = 3$ parametric comparison in the main manuscript by showing earlier stages of the same $\chi = 1$–5 evolution.

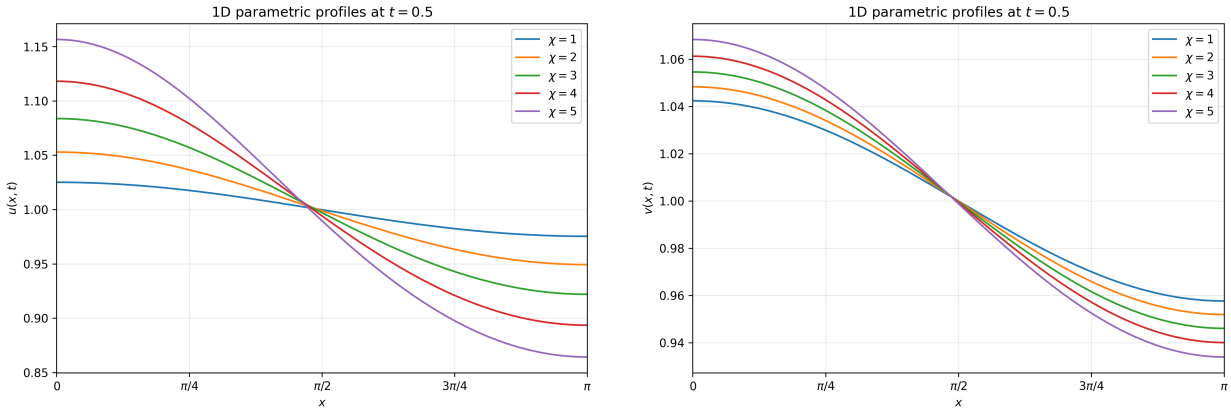


Figure S4: One-dimensional parametric profiles at $t = 0.5$: u (left) and v (right).

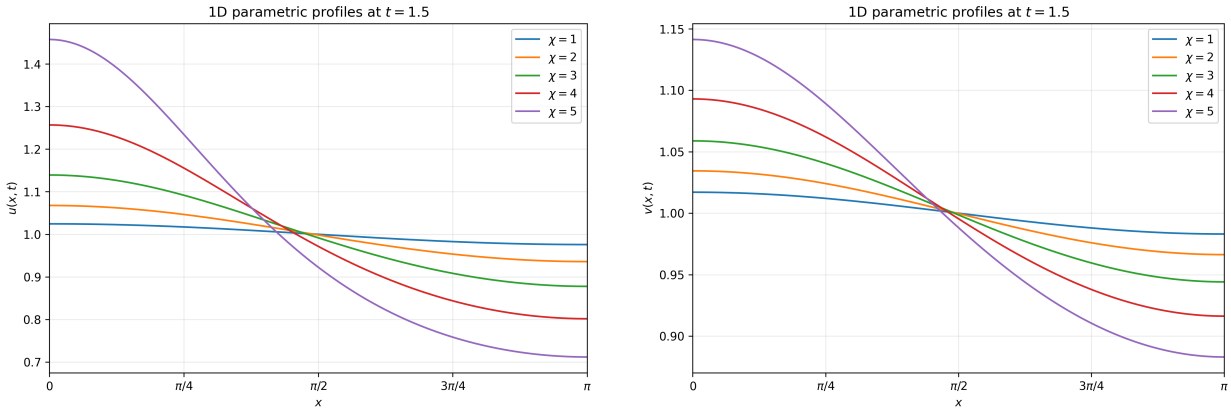


Figure S5: One-dimensional parametric profiles at $t = 1.5$: u (left) and v (right).

S3 Additional two-dimensional convergence and verification results

Table S3: Two-dimensional GITT errors at $t = 2$ for $N = 32$ relative to $N = 40$.

χ	$E_{\infty,U}$	$E_{2,U}$	$E_{\infty,V}$	$E_{2,V}$
1	3.239×10^{-10}	2.475×10^{-10}	3.740×10^{-10}	2.517×10^{-10}
2	1.982×10^{-9}	1.921×10^{-9}	3.761×10^{-9}	3.843×10^{-9}
3	7.737×10^{-10}	5.402×10^{-10}	4.780×10^{-10}	3.894×10^{-10}
4	2.074×10^{-9}	1.098×10^{-9}	1.208×10^{-9}	6.589×10^{-10}
5	4.769×10^{-7}	2.214×10^{-7}	3.266×10^{-9}	8.254×10^{-10}

Table S4: Reference-free two-dimensional FVM self-convergence orders at $t = 2$ for the $M = 40, 80, 160$ grid sequence.

χ	$p_{\infty,U}$	$p_{2,U}$	$p_{\infty,V}$	$p_{2,V}$
1	1.999520	1.999463	1.999283	1.999238
2	1.996484	1.996073	1.999456	1.999356
3	2.003309	2.001855	1.998253	1.998130
4	2.008355	2.001889	1.995573	1.999317
5	1.998721	1.999500	2.007529	2.000939

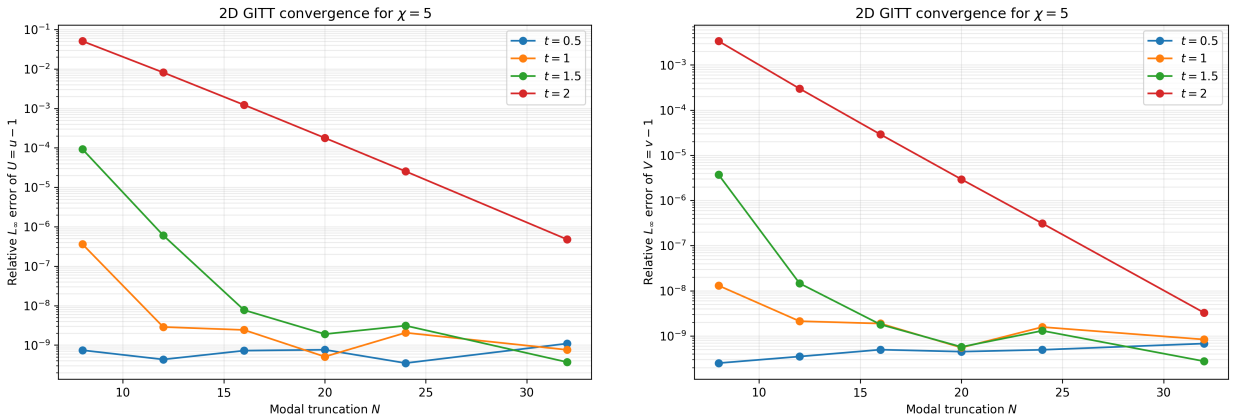


Figure S6: Two-dimensional GITT convergence for $\chi = 5$ at the four parametric times: U (left) and V (right).

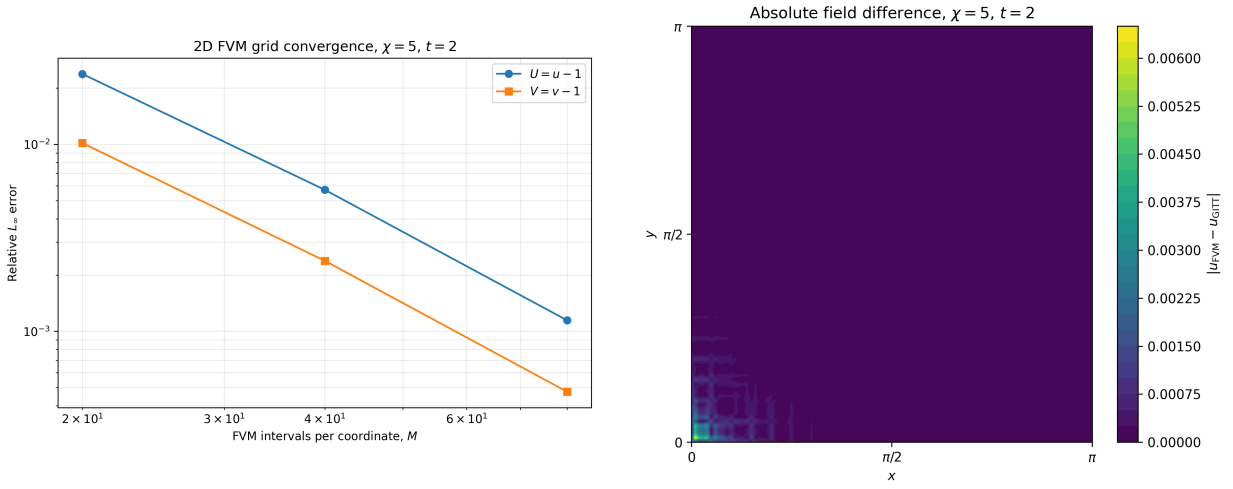


Figure S7: Independent two-dimensional FVM verification for $\chi = 5$, $t = 2$: FVM grid convergence (left) and absolute u-field difference relative to GITT (right).

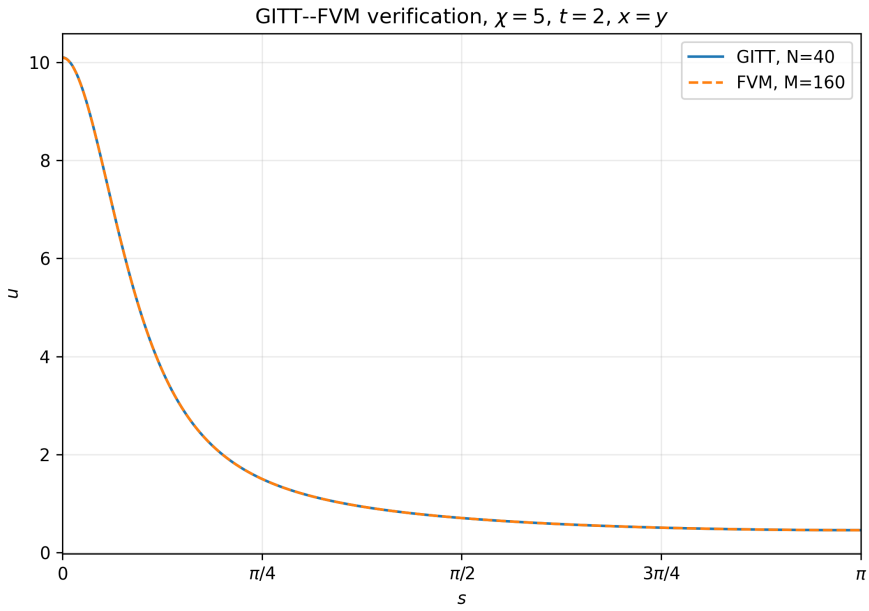


Figure S8: Additional GITT–FVM/MOL comparison for $\chi = 5$, $t = 2$: cell density along the diagonal cut $x = y$. The corresponding u- and v-field comparisons along $y = 0$ are reported in the main manuscript.

S4 Additional two-dimensional parametric visualization

These additional cuts and contour maps complement the peak-containing $y = 0$ profiles reported in the main manuscript and show the same parametric progression from alternative spatial views.

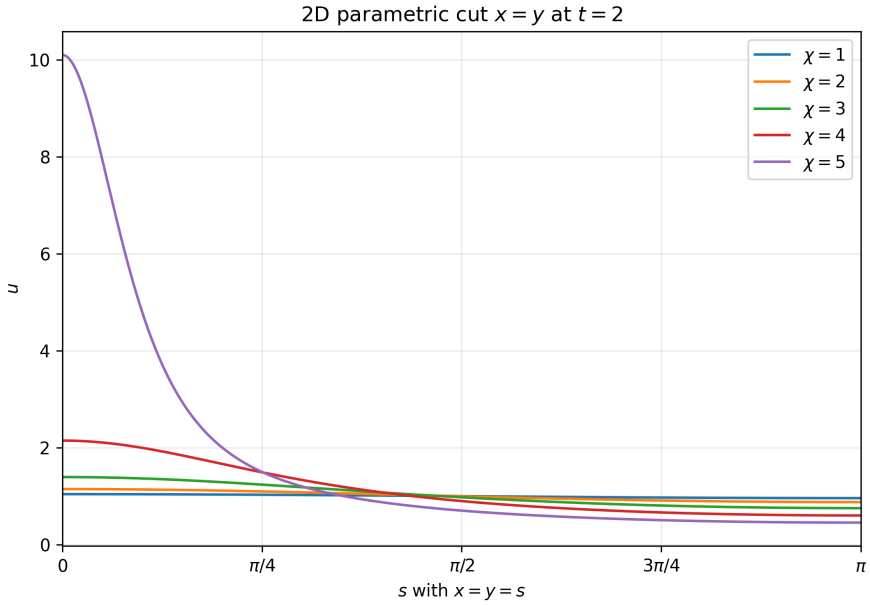


Figure S9: Two-dimensional GITT cell-density profiles along the diagonal cut $x = y$ at $t = 2$ for $\chi = 1$–5. The corresponding u- and v-profiles along $y = 0$ are reported in the main manuscript.

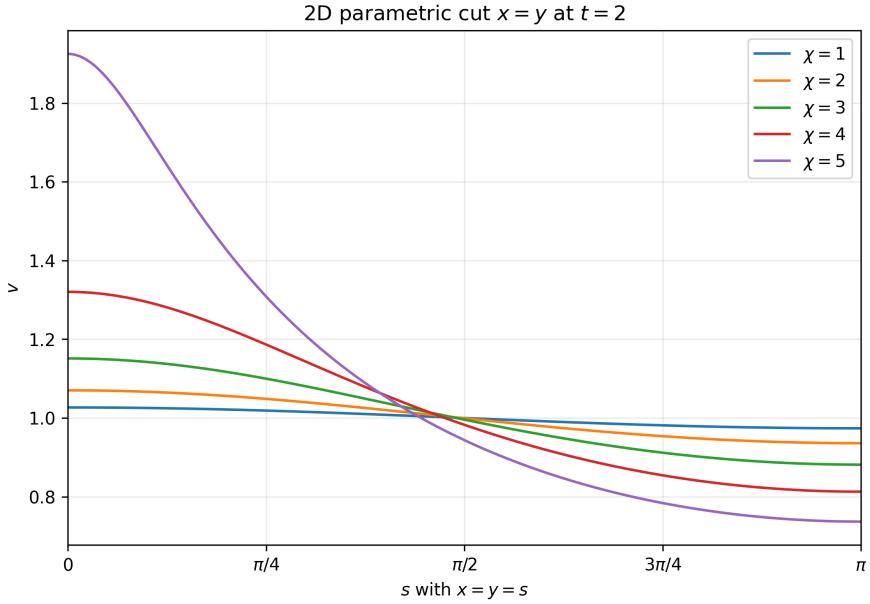


Figure S10: Two-dimensional chemoattractant profiles along $x = y$ at $t = 2$.

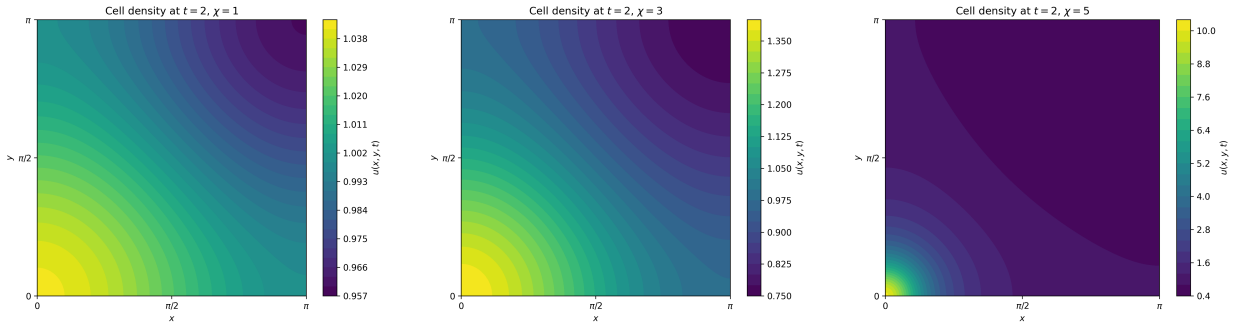


Figure S11: Cell-density contour maps at $t = 2$ for $\chi = 1$ (left), 3 (center), and 5 (right).

S5 Data-driven three-dimensional GITT surfaces at $t = 2$

The following surfaces are reconstructed directly from the converged $N = 40$ GITT modal solutions and provide a consistent visual comparison of the spatial response across the complete parametric set.

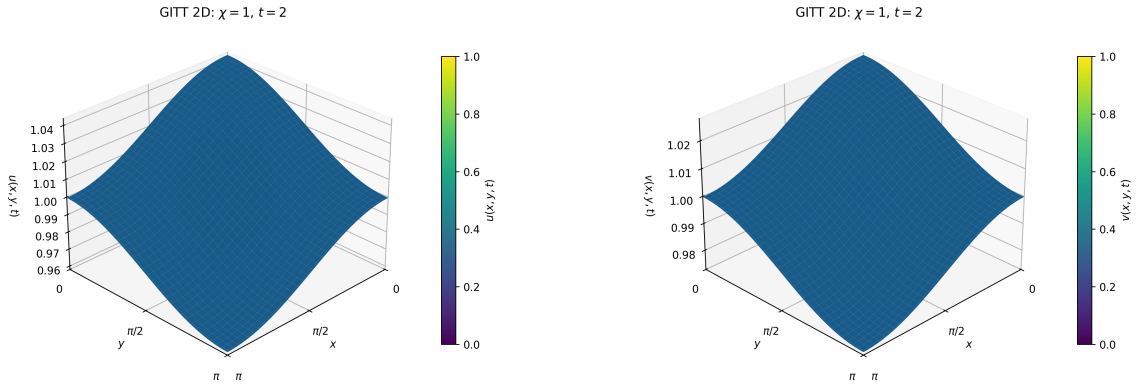


Figure S12: Three-dimensional GITT fields at $t = 2$ for $\chi = 1$: u (left) and v (right).

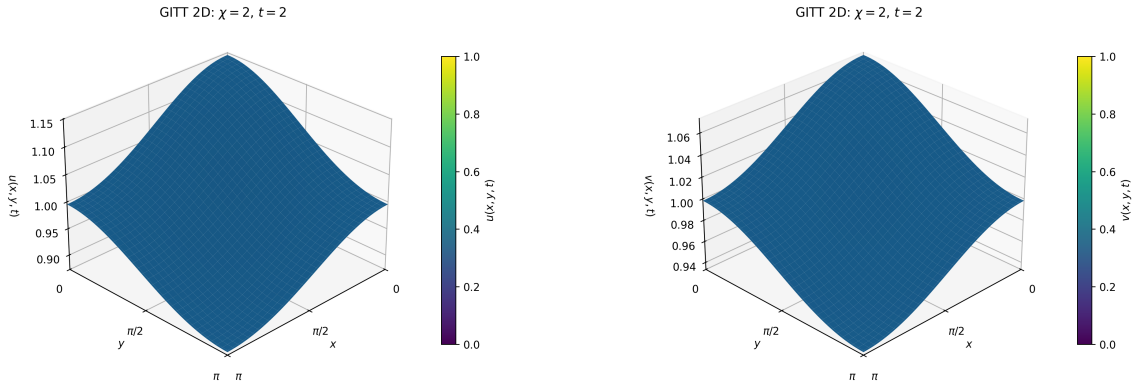


Figure S13: Three-dimensional GITT fields at $t = 2$ for $\chi = 2$: u (left) and v (right).

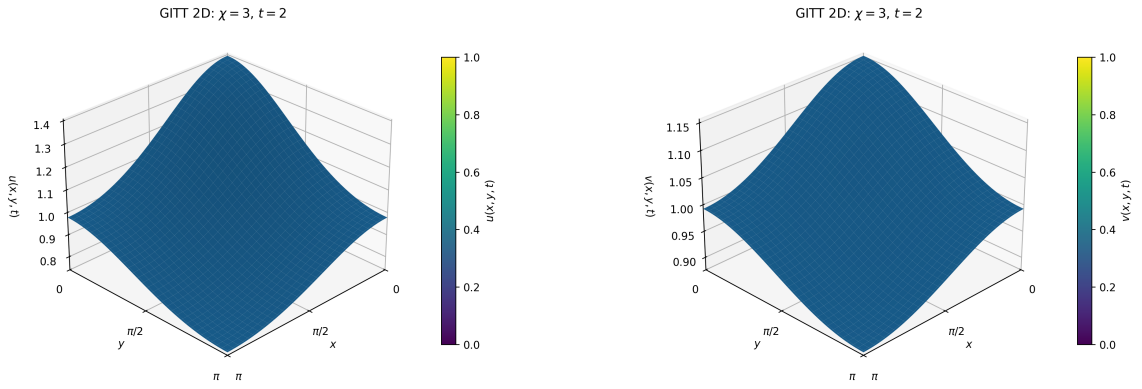


Figure S14: Three-dimensional GITT fields at $t = 2$ for $\chi = 3$: u (left) and v (right).

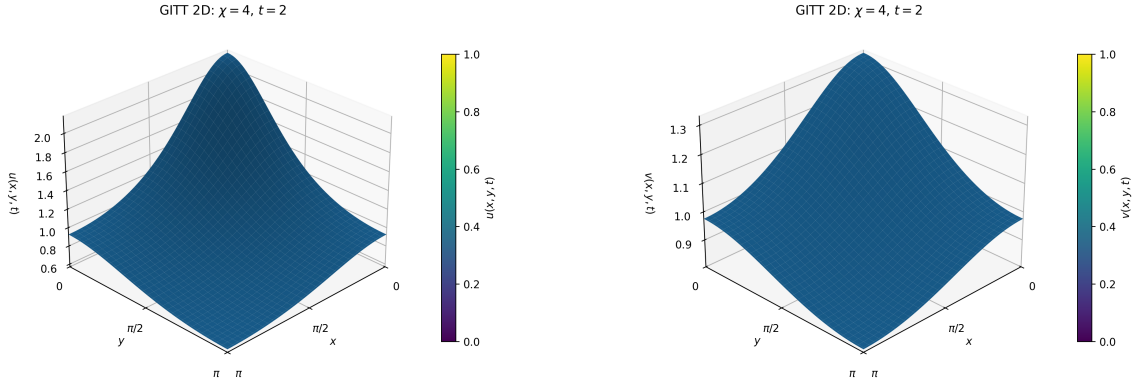


Figure S15: Three-dimensional GITT fields at $t = 2$ for $\chi = 4$: u (left) and v (right).

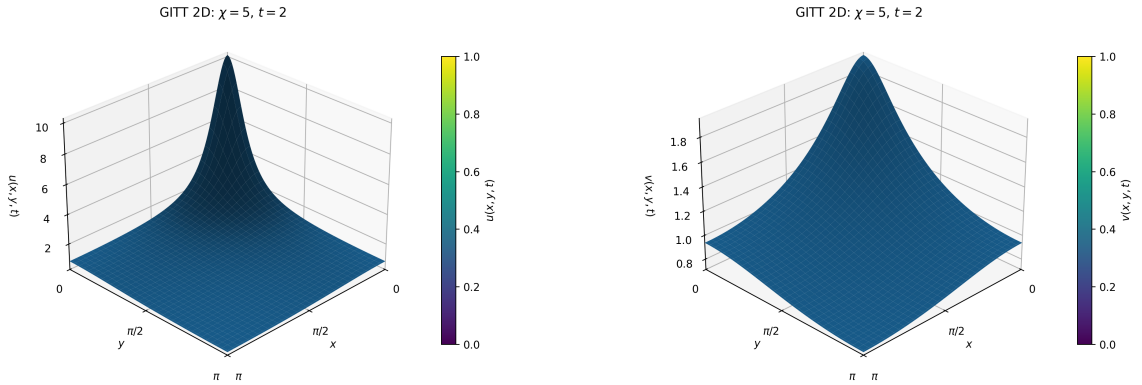


Figure S16: Three-dimensional GITT fields at $t = 2$ for $\chi = 5$: u (left) and v (right).